Electronic Supplementary Information

An organic transistor for detecting the oxidation of an organic sulfur compound at a solid-liquid interface and its chemical sensing applications

Yui Sasaki, [a,b] Yijing Zhang, [a] Kohei Ohshiro, [a] Kazuhiko Tsuchiya, [a] Xiaojun Lyu, [a] Masao Kamiko, [a] Yoshinori Ueno, [c] Hikaru Tanaka, [c] Tsuyoshi Minami *[a]

[a] Institute of Industrial Science, The University of Tokyo, 4-6-1 Komaba, Meguro-ku, Tokyo, 153-8505, Japan
Corresponding author: tminami@g.ecc.u-tokyo.ac.jp
[b] JST, PRESTO, 4-1-8 Honcho, Kawaguchi, Saitama, 332-0012, Japan
[c] Corporate Research Center, Toyobo Co., Ltd., 2-1-1 Katata, Otsu, Shiga, 520-0292, Japan

Contents

1. Fabrication and electronic characteristics of the OFET device

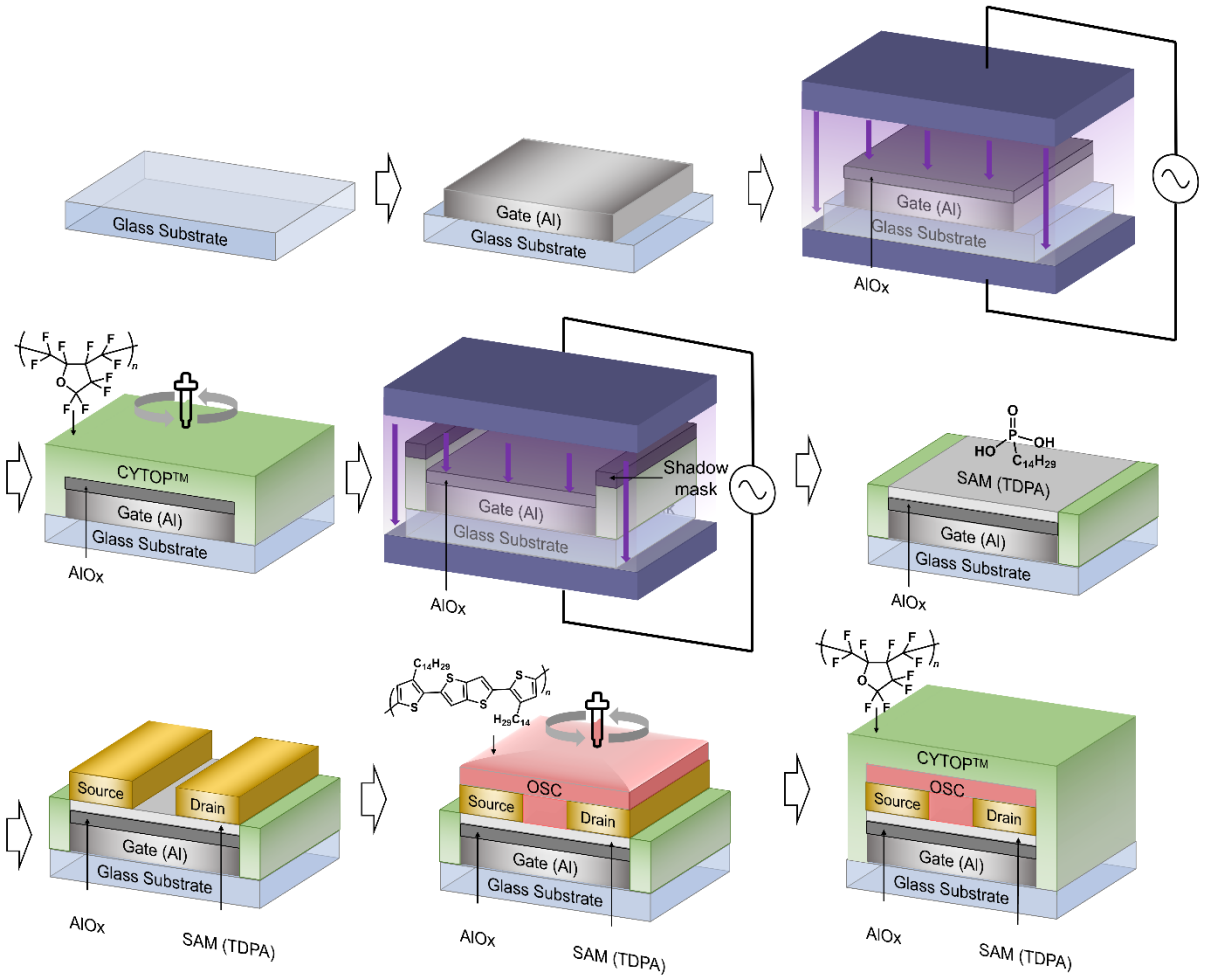

Fig. S1 Schematic illustration of the fabrication process of the OFET device.

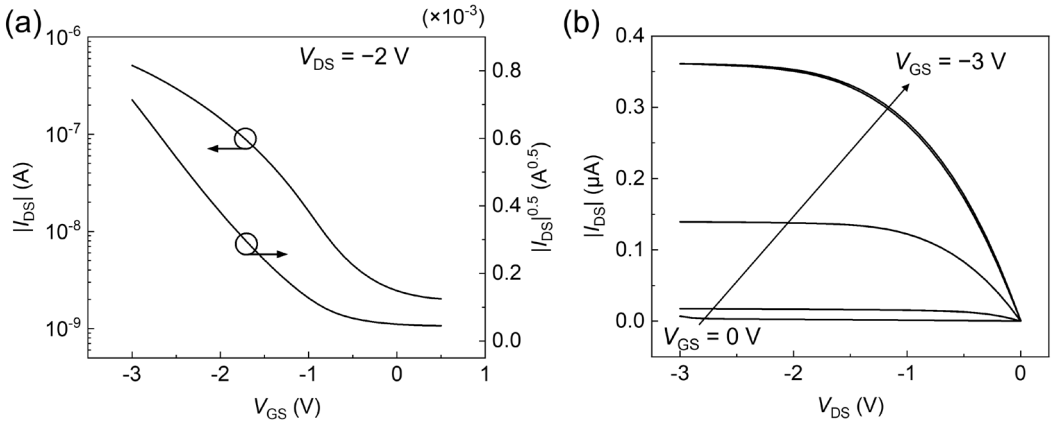

Fig. S2 (a) Transfer and (b) output characteristics of the OFET device.

2. Synthesis of 1,2-bis(4-{[4-(methylthio)phenyl]thio}phenyl)disulfane

Reagents

All reagents and samples were used without further purification. *N*,*N'*-dimethylformamide, ethyl acetate, sodium sulfate, and silica gel 60 (spherical) were purchased from Kanto Chemical Co. Ltd. Cesium carbonate was obtained from Tokyo Chemical Industry Co. Ltd. Tetra-*n*-butylammonium iodide was purchased from Sigma Aldrich Co. Iodomethane was purchased from Fujifilm Wako Pure Chemical Co.

Apparatuses

MALDI-TOF-MS: A JEOL JMS-S3000 SpiralTOF spectrometer was performed for matrix-assisted laser desorption/ionization time-of-flight type mass spectrometry (MALDI-TOF-MS). The sample was prepared by mixing 5 µL of a DMSO solution with 1,2-bis(4-{[4-(methylthio)phenyl]thio}phenyl)disulfane (1 mg/mL) and 20 µL of a DMSO solution with 2,5-dihydroxybenzoic acid as a matrix (10 mg/mL). The obtained sample solution and polyethylene glycol 400 as a standard sample for calibration were deposited on a 384-spots hairline-type plate with PEG400.

NMR: NMR measurements were conducted using a JEOL ECZ-600 spectrometer with solvent peaks or tetramethylsilane (TMS) as internal standards.

Melting point: Thermal analysis was performed by using BUCHI Melting Point B-545.

Synthesis of 1,2-bis(4-{[4-(methylthio)phenyl]thio}phenyl)disulfane

Under an N_2 atmosphere, cesium carbonate (0.820 g, 2.5 mmol) and tetra-*n*-butylammonium iodide (0.93 g, 2.5 mmol) were dissolved in *N*,*N'*-dimethylformamide anhydrous (13 mL) in a 50 mL two-necked round bottom flask. In this step, the freeze-pump-thaw method and N_2 replacement were applied to the solution three times. Afterward, 4,4'-thiobisbenzenethiol (0.63 g, 2.5 mmol) was added to the mixture and then cooled under 0 °C. After the dropwise addition of methyl iodide (390 mg, 2.75 mmol), the mixture was stirred for 1 h at 0 °C. Subsequently, the following procedure was carried out under ambient conditions. After the solution was quenched with 30 mL of deionized (DI) water at r.t., the product was extracted with 30 mL of ethyl acetate three times. In this process, the organic layer was washed with 30 mL of DI water three times. The obtained organic solution was dried over sodium sulfate. After the removal of the solvent *in vacuo*, the crude product was purified by using silica gel column chromatography (*n*-hexane:dichloromethane = 4:1–1:1, v/v). After the solvent was removed in *vacuo*, 1,2-bis(4-{[4-(methylthio)phenyl]thio}phenyl)disulfane (0.08 g, 12.1 %) was obtained. The collected product was further purified by using preparative thin-layer chromatography (silica gel 0.2 mm thickness, *n*-hexane:dichloromethane = 2:1, v/v).

^{1}H NMR (600 MHz, $CDCl_3$): δ(ppm) 7.35 (d, 4H, *J* = 8.4 Hz, -S-Ar*H*-S-S-Ar*H*-S-), 7.29 (d, 4H, *J* = 7.8 Hz, -S-Ar*H*-S-S-Ar*H*-S-), 7.19 (d, 4H, *J* = 8.4 Hz, CH_3S-Ar*H*), 7.14 (d, 4H, *J* = 8.4 Hz, CH_3S-Ar*H*), 2.47 (s, 6H, C*H*$_3$S-); ^{13}C NMR (151 MHz, $CDCl_3$): δ(ppm) 139.08, 136.82, 135.14, 133.10, 130.16, 129.99, 128.75, 127.17, 15.68;

HR MS (MALDI, +) *m/z*: Calcd. for $C_{26}H_{22}S_6$ 526.0040; Found: 526.0065, Δ_{error} 4.75 ppm; m.p. 112–113 °C.

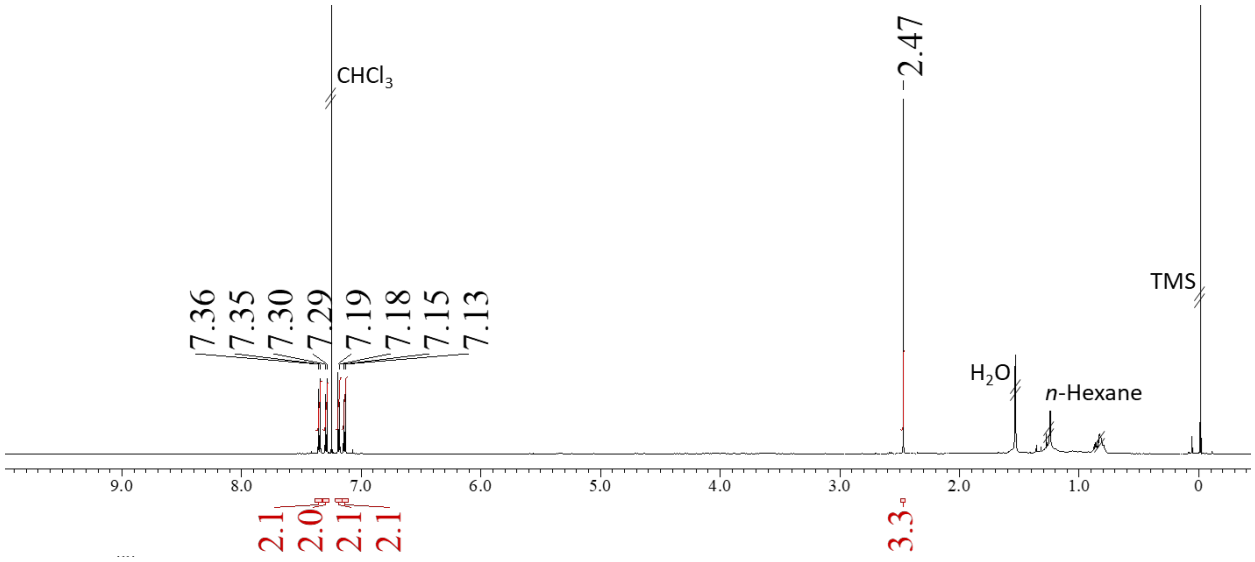

Fig. S3 ^{1}H NMR spectrum of 1,2-bis(4-{[4-(methylthio)phenyl]thio}phenyl)disulfane (600 MHz, $CDCl_3$) at 293 K.

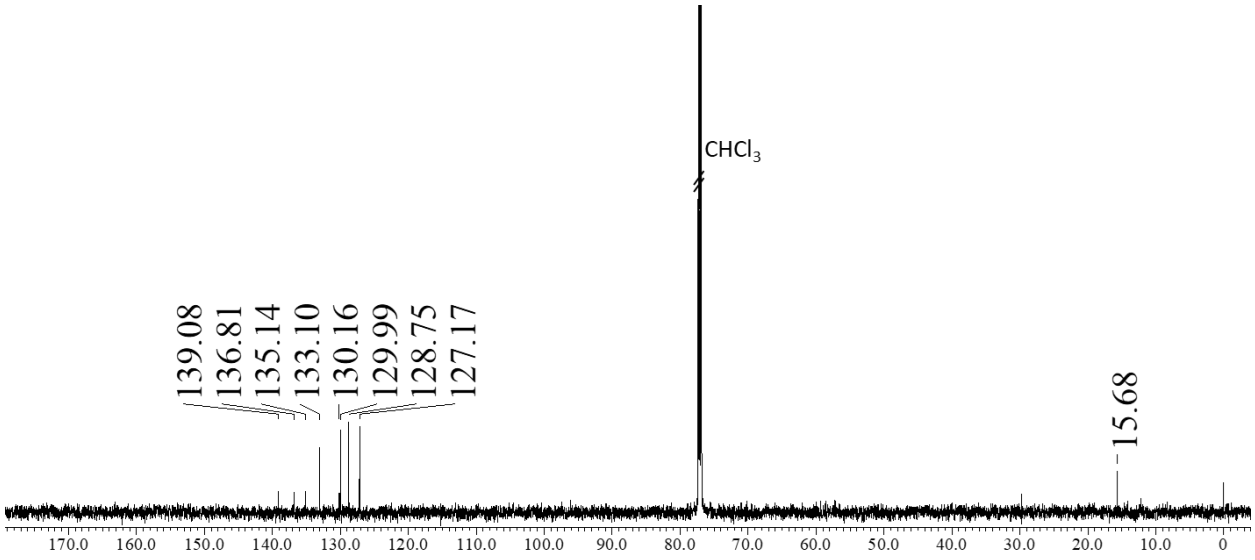

Fig. S4 ^{13}C NMR spectrum of 1,2-bis(4-{[4-(methylthio)phenyl]thio}phenyl)disulfane (151 MHz, $CDCl_3$) at 293 K.

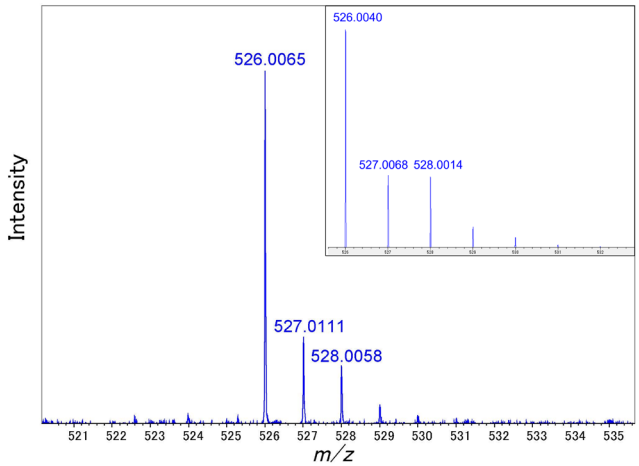

Fig. S5 MALDI-TOF-MS spectrum of 1,2-bis(4-{[4-(methylthio)phenyl]thio}phenyl)disulfane. The inset shows a calculated isotope pattern for $C_{26}H_{22}S_6$.

3. Characterization of the extended-gate electrode

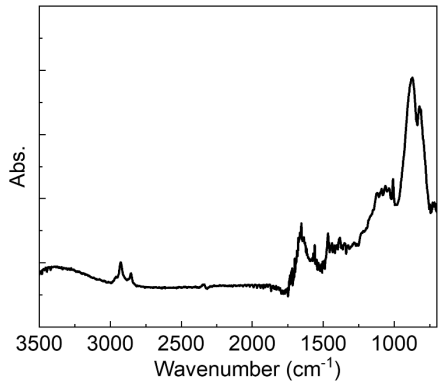

Fig. S6 FT-IR(ATR) spectrum of the 4,4'-thiobisbenzenethiol-modified extended-gate Au electrode.

4. Time-dependency test

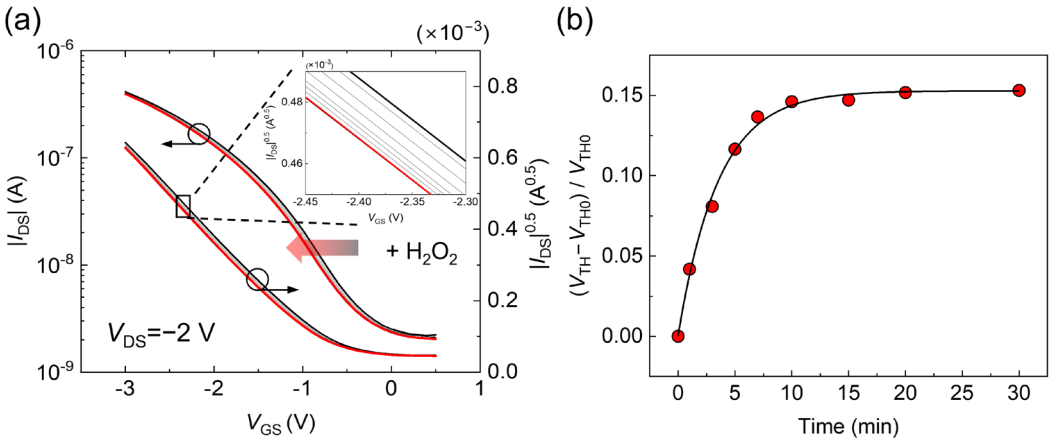

Fig. S7 (a) Transfer characteristics of the OFET device functionalized with 4,4'-thiobisbenzenethiol upon adding H_2O_2 (100 μM) in a HEPES (100 mM) buffer solution containing NaCl (100 mM) at pH 7.4. (b) Time-course change of the threshold voltages.

As shown in Fig. 5, the shifts of transistor characteristics were caused by the conversion of the thiol group into a disulfide structure shown in equation (1). Thus, we estimated an apparent reaction rate constant according to the following hypotheses; 1) an elementary reaction of equation (2) is assumed as the rate-determining step in the oxidation process,[S1] and 2) the concentration of H_2O_2 is much higher than that of R-SH ($[H_2O_2]$>>[R-SH]).

2R-SH + H_2O_2 ⟶ R-S-S-R + 2H_2O (1)

R-SH + H_2O_2 ⟶ R-SOH + H_2O (2)

$$\frac{d[R\text{-}S\text{-}S\text{-}R]}{dt} = k_a[H_2O_2]_0([R\text{-}SH]_0 - 2[R\text{-}S\text{-}S\text{-}R])$$

In [R-S-S-R], when t = 0 and [R-S-S-R] = 0,

$$\int \frac{1}{[R\text{-}SH]_0 - 2[R\text{-}S\text{-}S\text{-}R]} d[R\text{-}S\text{-}S\text{-}R] = \int k_a[H_2O_2]_0 dt$$

$$\frac{1}{2}(ln[R\text{-}SH]_0 - ln([R\text{-}SH]_0 - 2[R\text{-}S\text{-}S\text{-}R])) = k_a[H_2O_2]_0 t$$

$$\ln\left(1-\frac{2[R\text{-}S\text{-}S\text{-}R]}{[R\text{-}SH]_0}\right)=-2k_a[H_2O_2]_0t$$

$$1-\frac{2[R\text{-}S\text{-}S\text{-}R]}{[R\text{-}SH]_0}=e^{-2k_a[H_2O_2]_0t}$$

$$\frac{2[R\text{-}S\text{-}S\text{-}R]}{[R\text{-}SH]_0}=1-e^{-2k_a[H_2O_2]_0t}$$

$$[R\text{-}S\text{-}S\text{-}R]=\frac{[R\text{-}SH]_0}{2}\left(1-e^{-2k_a[H_2O_2]_0t}\right)$$

when t = 0, $[\text{R-S-S-R}]_0 = 0$,
and when $t = \infty$, $[\text{R-S-S-R}]_\infty = [\text{R-SH}]_0/2$

$$\ln\left(1-\frac{[R\text{-}S\text{-}S\text{-}R]}{[R\text{-}S\text{-}S\text{-}R]_\infty}\right)=-2k_a[H_2O_2]_0t$$

Therefore, a linear line by $\ln\left(1-\frac{[R\text{-}S\text{-}S\text{-}R]}{[R\text{-}S\text{-}S\text{-}R]_\infty}\right)$ can be obtained.

Using the time-course change of the threshold voltages (Fig. S7b), the correlation between the reaction time and the concentrations (Fig. S8) was obtained. By a linear fitting analysis, a slope was estimated to be -4.77×10^{-3}. Judging by a reaction rate constant in a previous report related to disulfide oxidation,[S1] the estimated k_a is a reasonable value.

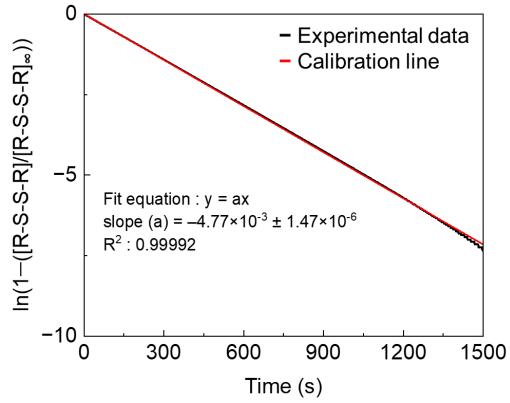

Fig. S8 The correlation between reaction time and concentrations.

5. Selectivity test

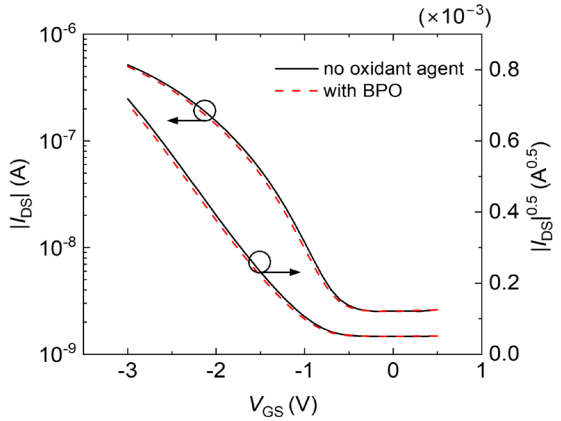

Fig. S9 Transfer characteristics of the OFET functionalized with 4,4'-thiobisbenzenethiol before and after adding benzoyl peroxide (BPO) (1 µM) in a HEPES (100 mM) buffer solution containing NaCl (100 mM) at pH 7.4.

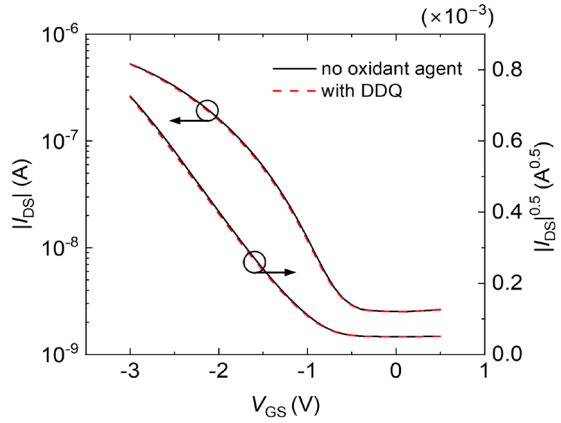

Fig. S10 Transfer characteristics of the OFET functionalized with 4,4'-thiobisbenzenethiol before and after adding 2,3-dichloro-5,6-dicyano-1,4-benzoquinone (DDQ) (1 µM) in a HEPES (100 mM) buffer solution containing NaCl (100 mM) at pH 7.4.

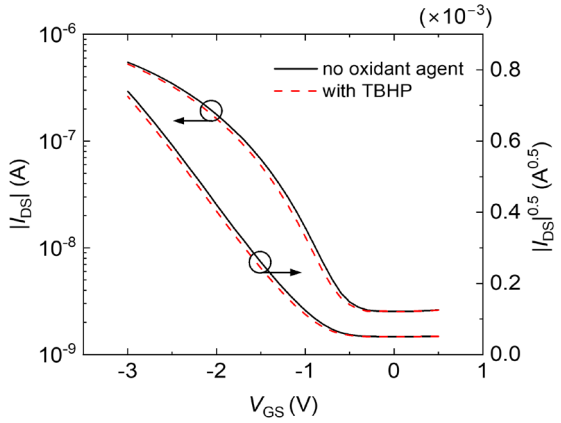

Fig. S11 Transfer characteristics of the OFET functionalized with 4,4'-thiobisbenzenethiol before and after adding *tert*-butyl hydroperoxide (TBHP) (1 µM) in a HEPES (100 mM) buffer solution containing NaCl (100 mM) at pH 7.4.

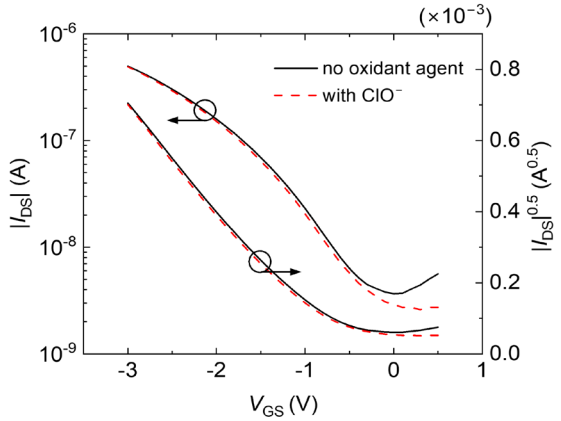

Fig. S12 Transfer characteristics of the OFET functionalized with 4,4'-thiobisbenzenethiol before and after adding sodium hypochlorite (1 µM) in a HEPES (100 mM) buffer solution containing NaCl (100 mM) at pH 7.4.

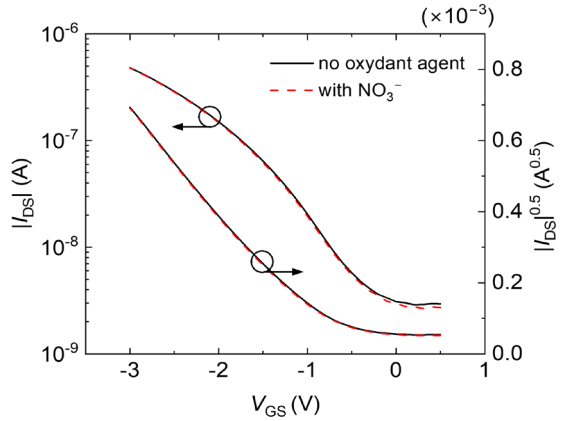

Fig. S13 Transfer characteristics of the OFET functionalized with 4,4'-thiobisbenzenethiol before and after adding sodium nitrate (1 µM) in a HEPES (100 mM) buffer solution containing NaCl (100 mM) at pH 7.4.

6. Surface analysis

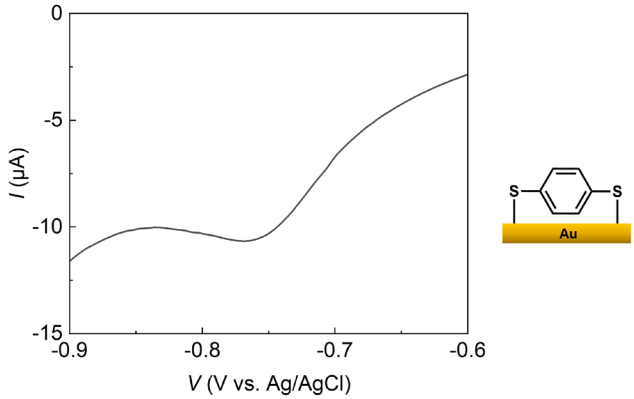

Fig. S14 Result of the molecular density estimation by using LSV. The evaluation of the extended-gate electrode functionalized with 1,4-benzenedithiol was performed in a KOH solution (0.1 M). The potential was applied from 0 V to −1.5 V, and the scan rate was set to 20 mV/s. The molecular density of 1,4-benzenedithiol on the extended-gate electrode was determined based on Faraday's law with the integration of the peak area. The molecular density of 1,4-benzenedithiol was estimated to be (8.70 ± 1.52) ×10^{-10} mol/cm^2 (n = 5).

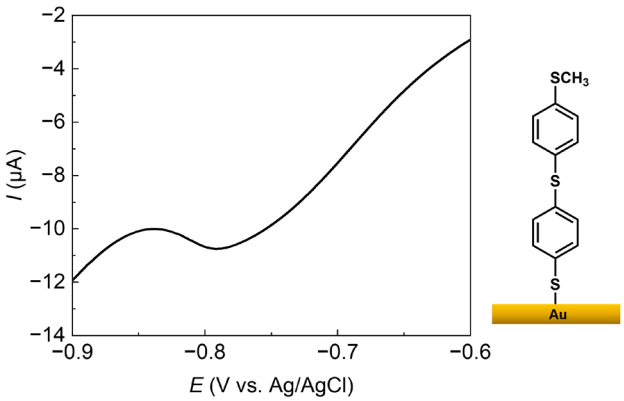

Fig. S15 Result of the molecular density estimation by using LSV. The evaluation of the extended-gate electrode functionalized with 4-{[4-(methylthio)phenyl]thio}benzenethiol was performed in a KOH solution (0.1 M). The potential was applied from 0 V to −1.5 V, and the scan rate was set to 20 mV/s. The molecular density of 4-{[4-(methylthio)phenyl]thio}benzenethiol on the extended-gate electrode was determined based on Faraday's law with the integration of the peak area. The molecular density of 4-{[4-(methylthio)phenyl]thio}benzenethiol was estimated to be (7.70 ± 0.42) $\times 10^{-10}$ mol/cm^2 (n = 5).

7. EI MS analysis

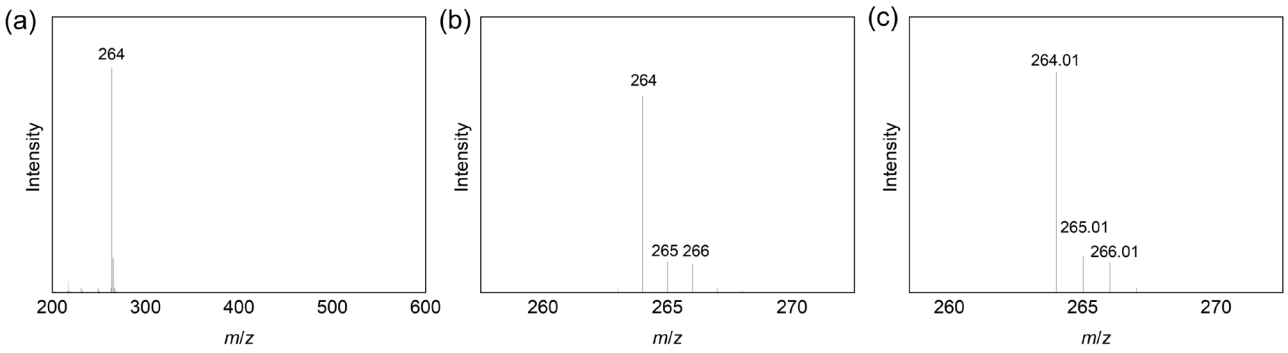

Fig. S16 EI MS spectra of 4-{[4-(methylthio)phenyl]thio}benzenethiol (2 mM) with TCEP (5 mM) in DMSO before H_2O_2 treatment. (a) A wide range of the MS spectrum. (b) MS (EI, +) m/z: 264 $M^{+\bullet}$ (c) Calculated isotope patterns for $C_{13}H_{12}S_3$ 264.01.

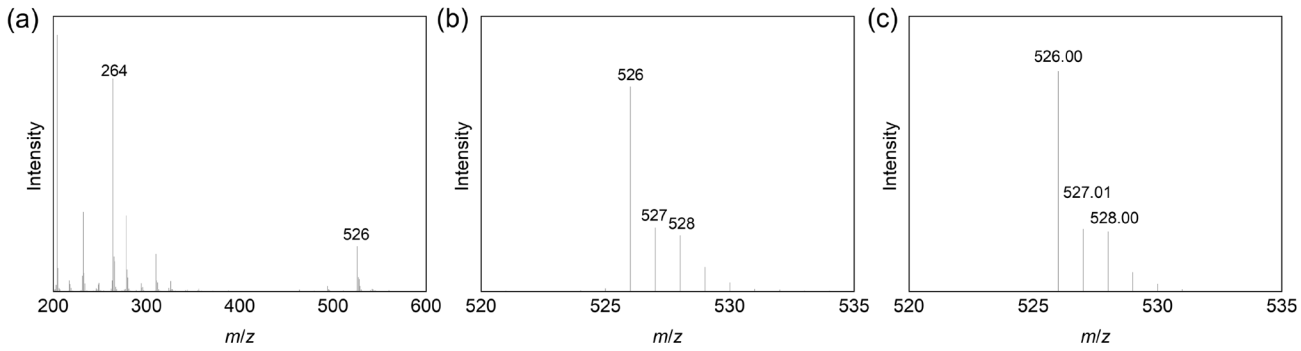

Fig. S17 EI MS spectra of 4-{[4-(methylthio)phenyl]thio}benzenethiol (2 mM) with TCEP (5 mM) in DMSO after H_2O_2 (100 mM) treatment. (a) A wide range of the MS spectrum. (b) MS (EI, +) m/z: 526 $[2M-2H]^{+\bullet}$. (c) Calculated isotope patterns for $C_{26}H_{22}S_6$ 526.00.

8. DFT calculations

The DFT calculations were operated by using Gaussian 16 Revision C.01.[S2] The structures of Fig. S18(a) and (b) were optimized and calculated at the B3LYP(D3BJ)/def2SVP[S3-S6] level for generating the wave function files, which was further analyzed with Multiwfn 3.8.[S7,S8] The calculated dipole moments were visualized by Visual Molecular Dynamics (VMD) 1.9.4.[S9]

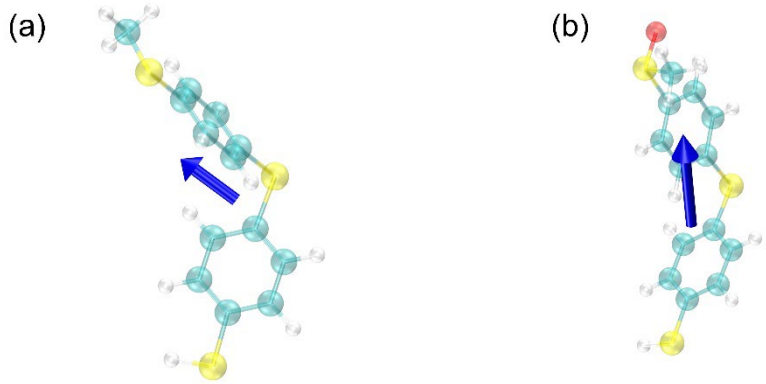

Fig. S18 DFT calculation results of the dipole moment of (a) 4,4'-thiobisbenzenethiol and (B) the oxidized structure.

9. XPS analysis

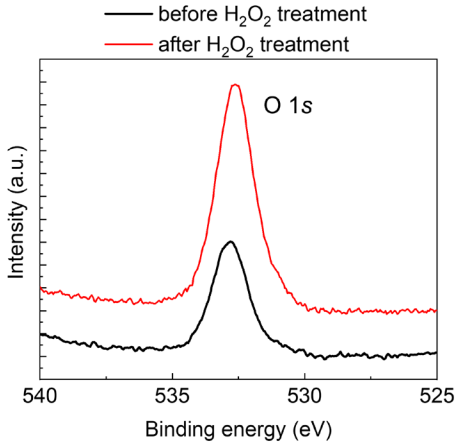

Fig. S19 XPS spectra of O 1*s* region for the extended-gate Au electrode functionalized with 4,4'-thiobisbenzenethiol before (black line) and after H_2O_2 treatment (red line). The relative atomic concentration ratio of ([O] / [S] + [O]) was determined to be ca. 56% and ca. 77% before and after H_2O_2 treatment, respectively.

10. Real-time monitoring of transistor responses in the absence of lactate oxidase

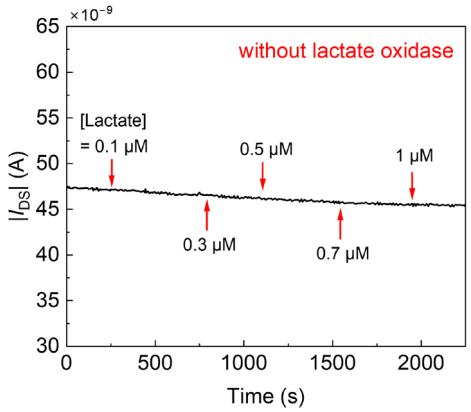

Fig. S20 Real-time monitoring of transistor responses upon adding lactate in the absence of lactate oxidase in a D-PBS solution.

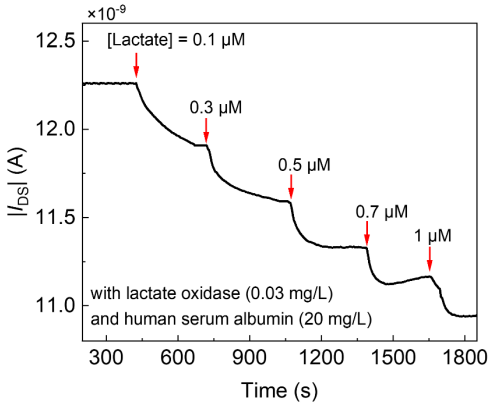

Fig. S21 Real-time monitoring of transistor responses upon adding lactate in the presence of lactate oxidase in a D-PBS solution. [Lactate oxidase] = 0.03 mg/L, [lactate] = 0–1 μM, [human serum albumin] = 20 mg/L.V_{GS} = V_{DS} = −2 V.

References

S1. Z. Abedinzadeh, M. Gardes-Albert and C. Ferradini, Can. J. Chem., 1989, **67**, 1247-1255.

S2. M. J. Frisch, G. W. Trucks, H. B. Schlegel, G. E. Scuseria, M. A. Robb, J. R. Cheeseman, G. Scalmani, V. Barone, G. A. Petersson, H. Nakatsuji, X. Li, M. Caricato, A. V. Marenich, J. Bloino, B. G. Janesko, R. Gomperts, B. Mennucci, H. P. Hratchian, J. V. Ortiz, A. F. Izmaylov, J. L. Sonnenberg, D. Williams-Young; ; F. Ding, F. Lipparini, F. Egidi, J. Goings, B. Peng, A. Petrone, T. Henderson, D. Ranasinghe, V. G. Zakrzewski, J. Gao, N. Rega, G. Zheng, W. Liang, M. Hada, M. Ehara, K. Toyota, R. Fukuda, J. Hasegawa, M. Ishida, T. Nakajima, Y. Honda, O. Kitao, H. Nakai, T. Vreven, K. Throssell, J. A. Jr. Montgomery, J. E. Peralta, F. Ogliaro, M. J. Bearpark, J. J. Heyd, E. N. Brothers, K. N. Kudin, V. N. Staroverov, T. A. Keith, R. Kobayashi, J. Normand, K. Raghavachari, A. P. Rendell, J. C. Burant, S. S. Iyengar, J. Tomasi, M. Cossi, J. M. Millam, M. Klene, C. Adamo, R. Cammi, J. W. Ochterski, R. L. Martin, K. Morokuma, O. Farkas, J. B. Foresman and D. J. Fox, Gaussian 16 (Revision. C.01), Gaussian Inc., Wallingford, CT, 2016 (accessed February 28, 2022).

S3. A. D. Becke, *Phys. Rev. A*, 1988, **38**, 3098-3100.

S4. A. D. Becke, *J. Chem. Phys.*, 1993, **98**, 5648-5652.

S5. C. Lee, W. Yang and R. G. Parr, *Phys. Rev. B*, 1988, **37**, 785-789.
S6. S. Grimme, J. Antony, S. Ehrlich and H. Krieg, *J. Chem. Phys.*, 2010, **132**, 154104.
S7. B. P. Pritchard, D. Altarawy, B. Didier, T. D. Gibson and T. L. Windus, *J. Chem. Inf. Model*., 2019, **59**, 4814-4820.
S8. T. Lu and F. Chen, *Comput. Chem.*, 2012, **33**, 580-592.
S9. W. Humphrey, A. Dalke and K. Schulten, *J. Mol. Graphics*, 1996, **14**, 33-38.